

Available online at www.sciencedirect.com

jmr&t
Journal of Materials Research and Technology
journal homepage: www.elsevier.com/locate/jmrt



Review Article

Energy absorption capability of graded and non-graded sheet-based gyroid structures fabricated by microcast processing[☆]



Leonie Wallat ^{a,b,*}, Michael Selzer ^{b,c}, Uwe Wasmuth ^a, Frank Poehler ^a, Britta Nestler ^{b,c,2}

^a Institute of Materials and Processes, Karlsruhe University of Applied Sciences, Moltkestr. 30, 76133 Karlsruhe, Germany

^b Institute for Digital Materials Research, Karlsruhe University of Applied Sciences, Moltkestr. 30, 76133 Karlsruhe, Germany

^c Institute for Applied Materials - Microstructure Modeling and Simulation, Karlsruhe Institute of Technology, Kaiserstraße 12, 76131 Karlsruhe, Germany

ARTICLE INFO

Article history:

Received 27 July 2022

Accepted 25 September 2022

Available online 11 October 2022

Keywords:

Sheet-based gyroid

Graded structure

Microcast processing

Mechanical analysis

ABSTRACT

This review analyses the design, manufacture and mechanical behaviour of sheet-based gyroid structures with different gradients, made of the alloy AlSi7Mg0.6. Contrary to most contributions, additive manufacturing was not used for the production of the metallic lattices. The lattices were manufactured by microcast processing, which represents an alternative manufacturing option for complex structures. Five different gyroid structures of AlSi7Mg0.6, with a porosity between 40% and 80% and different gradients, are produced and analysed. The special feature here is that, in addition to constant and linear gradients, a non-linear gradient is also taken into account. With the introduction of a non-linear gradient, a hardly considered structure is introduced. By introducing new gradients, the structures can be better adapted to their environment.

The main focus of the mechanical behaviour analysis was on the possible energy absorption capacity. For this purpose, compression tests were performed. The plateau of the resulting stress–strain diagram of structures with constant porosities of 80% and 60% characterises an ideal course for energy absorption. However, graded porosity structures with porosities ranging from 80% to 40% have a higher energy absorption capacity than the structures with a constant porosity of 80%. The results show a new possibility that a targeted adjustment of the energy absorption potential is possible through future topology optimisation, which would be attractive in industries with crash safety areas.

© 2022 The Author(s). Published by Elsevier B.V. This is an open access article under the CC BY license (<http://creativecommons.org/licenses/by/4.0/>).

[☆] This document contains the results of the research project: “Innovative Schaumstrukturen für effizienten Leichtbau” and results of the research project “Mittelbau”.

* Corresponding author.

E-mail address: leonie.wallat@h-ka.de (L. Wallat).

¹ www.h-ka.de, Karlsruhe University of Applied Sciences (L. Wallat).

² www.kit.edu, Karlsruhe Institute of Technology (B. Nestler).

<https://doi.org/10.1016/j.jmrt.2022.09.093>

2238-7854/© 2022 The Author(s). Published by Elsevier B.V. This is an open access article under the CC BY license (<http://creativecommons.org/licenses/by/4.0/>).

1. Introduction

In engineering applications, lattice structures are often used to obtain lighter and high-strength materials. These structures are often copied from nature, which has produced efficient cell structures that are characterised by high stiffness and strength, such as the bones, woods, or teeth. These structures are also known as natural energy absorbers. A characteristic property of natural structures is the fact that they often have a complex shape with a density gradient [1,2].

An example of a complex structure that occurs in nature, but does not necessarily have a density gradient, is the gyroid structure, which belongs to the family of triply periodic minimal surfaces (TPMS) [3]. In general, TPMS can be defined by mathematical functions that allow the adjustment of various parameters such as the cell size, the number of cells and the porosity. They are characterised by the fact that the mean curvature is zero at every point on the surface. This results in a complex shape, a non-intersecting curved surface, that repeats periodically in all directions [4,5]. These structures can be based on either polymers or metals [6]. Due to this complex shape, additive manufacturing (AM), such as selective laser powder bed fusion technology [7], fused filament fabrication [8], electron beam melting [9] or selective laser sintering [10], is predominantly used. Their complex shape, copied from nature, makes the structures interesting for a wide variety of

research applications and areas. Their topology, for example, is similar to that of trabecular bones, which means that the TPMS structures are attracting attention in the field of tissue engineering [11].

In the topology of the gyroid structure, a distinction is made between sheet-based and strut-based structures [12]. A key difference between the two types of topology is that the sheet-based structures have a larger surface-to-volume ratio and a two-chamber system [13]. In Fig. 1, the respective chamber system of the strut-based gyroid (1 a.2) and the sheet-based gyroid (1 b.2) is marked.

In addition, various studies have shown that the mechanical properties of sheet-based gyroid structures are better than those of strut-based structures [7,14,15]. For this reason, this study focuses on sheet-based gyroid structures. The fact that it is reproduced by its mathematical formulation is a major advantage of the cell structure. The approximation formula of the sheet-based gyroid structure (hereafter called gyroid) is presented in equation (1) [16].

$$0 = \left[\sin \frac{2\pi x}{L_x} \cdot \cos \frac{2\pi y}{L_y} + \sin \frac{2\pi y}{L_y} \cdot \cos \frac{2\pi z}{L_z} + \sin \frac{2\pi z}{L_z} \cdot \cos \frac{2\pi x}{L_x} \right]^2 - t^2, \tag{1}$$

with the number of cell repetitions in the x-, y- and z- direction and the size of the unit cells (L_x, L_y, L_z) [17–19]. In

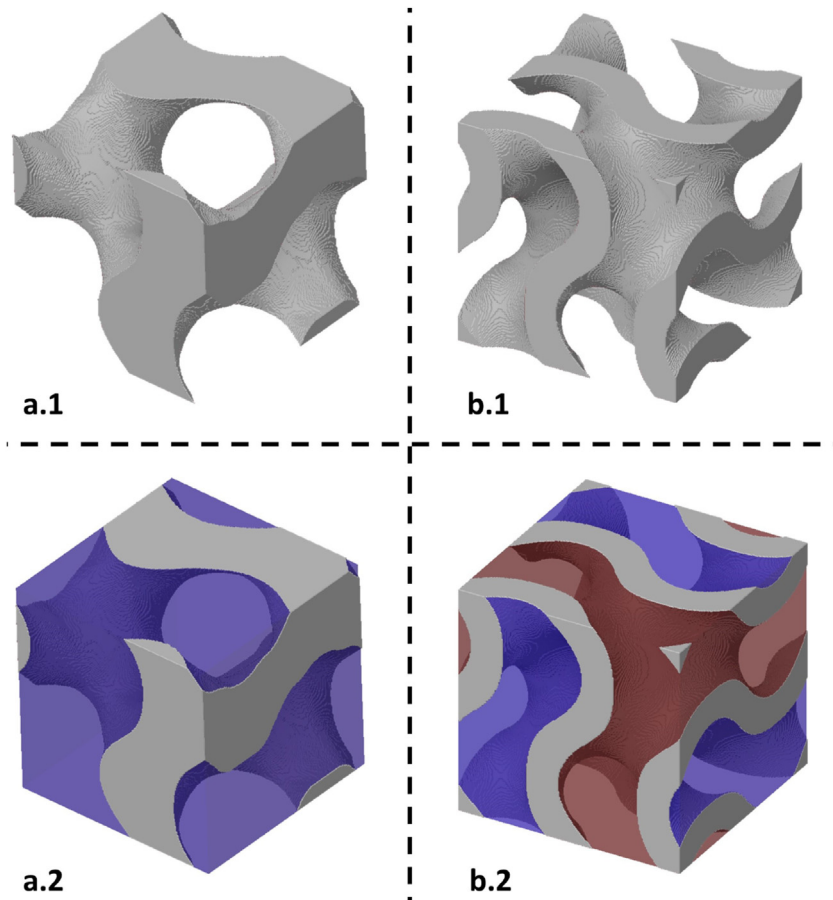


Fig. 1 – Strut-based (a) and sheet-based (b) gyroid with marked chamber system.

addition, the parameter (t) controls the wall thickness, which has a direct influence on the volume fraction (v^*) of the pore phase and the porosity (Φ) of the solid phase [20,21]. Φ is calculated according to the following equation [22,23]:

$$\Phi = (1 - v^*) \cdot 100\%, \quad (2)$$

with

$$v^* = \frac{v}{v_s}, \quad (3)$$

where v^* is defined by v , the volume of the pore structure, and v_s , the volume of the solid structure. The relationship between v^* and Φ is inverse, which means that a high porosity implies a low wall thickness. This relationship is illustrated in Fig. 2. For this purpose, three gyroid unit cells with porosities of 40%, 60% and 80% are shown. The above parameters have a significant influence on the mechanical properties [24].

The research and application areas of gyroid structures are diverse. Their two-chamber system and high surface-to-volume ratio favour applications where two media must interact separately [25], an example of which is a heat exchanger [26]. Another frequently considered area of research is the consideration of gyroid structures as possible crash structures. For this purpose, their energy absorption capacity is considered [27]. However, the structures under consideration are often characterised by uniform porosity [15,20,27,28].

When structures with gradients are considered, the gradients in cell size or porosity are usually in the linear range [18,19,29]. The possible applications and areas of research involving the use of gradient structures are diverse and promising. Liu [19] used linearly graded cell size gradients to mimic the natural environment of bone. In addition to Liu's work, other research has introduced linearly graded pore structures to achieve the best fit to the application domain. Dawei Li ([18]), for instance, has taken a closer look at the energy absorption potential of sheet-based and strut-based gyroid structures. It has been shown that the graded, sheet-based cellular structures have a better energy absorption capacity than the uniform and strut-based structures, which can be confirmed by Zhang et al. [30]. In Zhang's study [30], sheet-based gyroid structures with constant and linear profiles were analysed. The linear profile structures exhibit a more stable and longer plateau phase as well as a higher energy absorption capacity. Under compressive loads, the structures can additionally achieve a larger damping ratio than structures with constant porosity.

Despite the wide range of applications of gradient structures, non-linear gradients are rarely found in research. In [31], the energy absorption of lattice structures with linear and quadratic gradients (I-Wrapped Package, IW-P) is investigated in comparison to uniform structures. It can be seen that the structures with linear and quadratic gradients have a higher energy absorption capacity, when exposed to a greater load. This result highlights the fact that the introduction of non-linear gradients is promising. A widely considered topic is the control of the energy absorption capacity. In vehicle safety, for example, thin-walled structures are usually used as impact energy absorption elements. However, these can still be improved in terms of their structural configurations to

maximize occupant safety [32,33]. Since the good energy absorption behaviour of gyroid structures has already been shown in several studies [18,20,27], it is now interesting to consider the behaviour of gyroid structures with non-linear gradients, which is part of this work.

Since non-linear gradients have hardly been considered in research papers so far, this research area is still very new and offers a lot of potential. In addition to the study of energy absorption, another possibility for the use of non-linear gradients is the adaptation to the environment, for example, to the bone environment. Furthermore, better application-specific adjustments could be possible through non-linear gradients. In this work, the focus is on the study of energy absorption. For this purpose, gyroid structures with linear, quadratic and constant gradients with porosities in the range of 40%–60% are fabricated by microcast processing and are investigated by compression tests. Thereby, the fabrication of the structure represents a novelty. Usually, the structures are fabricated using additive manufacturing processes. Microcast processing is an alternative to the typical additive manufacturing processes for both complex and simple structures between 0.01 g and 30 g.

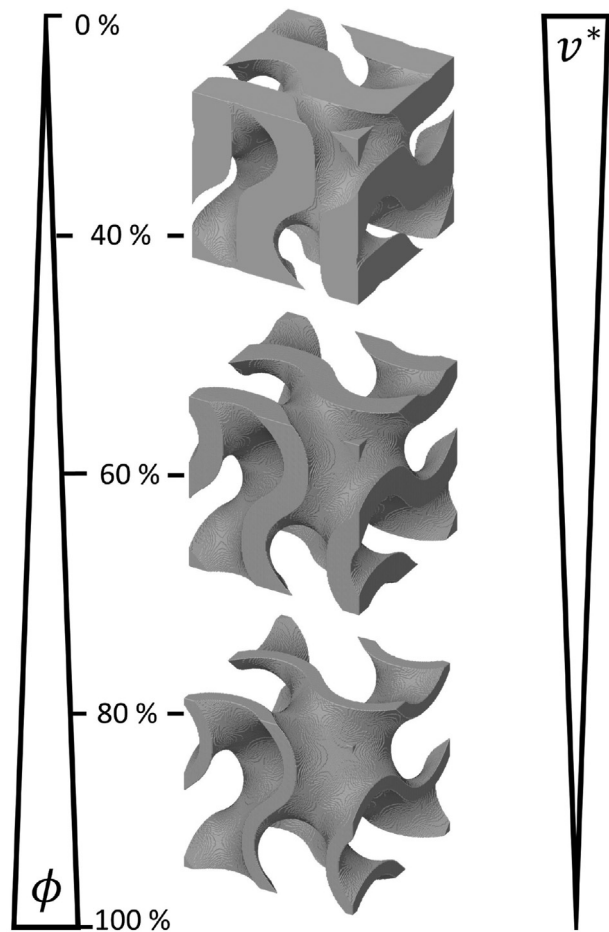


Fig. 2 – Contrary dependence between the porosity Φ and the volume fraction v^* : as the porosity increases, the volume fraction decreases. Illustrated on gyroid unit cells with a porosity of 40%, 60% and 80%.

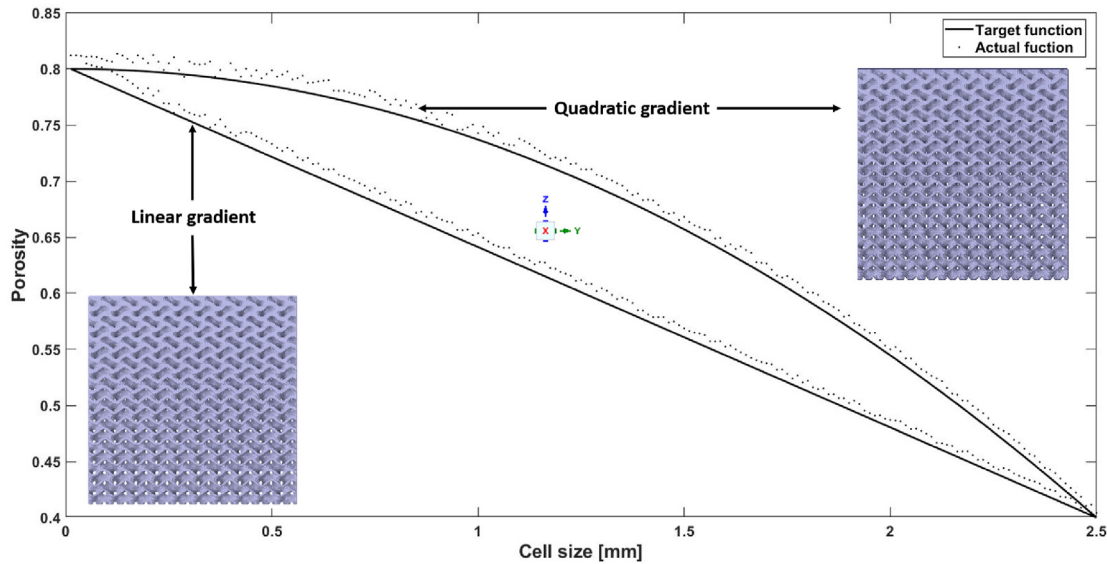


Fig. 3 – Function curve of gyroid structures with a linear and quadratic porosity of the actual (points) and target porosity function (line).

2. Structure generation

The structures are generated with the help of a self-programmed MatLab code [34]. For structures with gradients, a maximum (starting) porosity and a minimum (target) porosity are specified. Starting from the maximum porosity, the structure is thickened in either a linear or quadratic progression. The quadratic progression represents a quasi inverted parabola (see Fig. 3). The diagram shows the target and actual function of the structure, with a linear and quadratic porosity gradient over the cell size (x-axis) and the porosity (y-axis). Here, the actual and target porosity deviate slightly from each other. The course of the function shows that the structure with the quadratic gradient is thickened more slowly than the structure with the linear gradient. The thickening of the structures takes place in the z-direction. The specimens have a size of $25 \times 25 \times 25 \text{ mm}^3$, with 10 cells per spatial direction. The article by Wallat et al. [35] provides more detailed information about the MatLab code.

For the following analysis, the sample dimensions and test method are based on the international standard ISO 13314:2011 [36]. Samples with porosities from 40% to 80%, with a quadratic and linear gradient, and with a constant porosity of 40%, 60% and 80% are generated. Table 1 shows the calculated porosity from the stl files. Formula 2 is used to calculate the porosity.

As shown in Table 1, three samples within a similar porosity range (linear 40–80, quadratic 40–80 and constant 60) are compared. The structures with a constant porosity of 60% and the structures with linear porosities from 40% to 80% theoretically have an average equal porosity of 60%. The average porosity of the structures with a quadratic gradient is slightly higher than 60%, which is due to the fact that the structures with a quadratic gradient thicken more slowly, as shown by the quadratic gradient function in Fig. 3. In general, the porosity calculated from the stl files deviates from the

theoretical porosity by up to 4 percentage points. On the one hand, this is caused by the slight deviation that occurred during the generation of the structures and, on the other hand, by the tessellation of the stl files, which affects the accuracy [37]. In addition, the two extreme values ‘constant 40’ and ‘constant 80’ are considered.

3. Microcast processing

In addition to additive manufacturing processes such as selective laser melting (SLM) or selective laser sintering (SLS), generative microcast processing can also be used to manufacture complex components. This method offers the possibility to produce primitive and very complex structures, such as TPMS structures, with a wall thickness of at least 0.12 mm in large quantities, in a weight range between 0.01 g to approximately 30 g. Furthermore, it is suitable for the development and prototype phase of a product, as different geometry, design and material variants of a product can be produced in one manufacturing step. The special feature is that the original metal alloy such as copper-based, aluminium and zinc alloys or steels are used for the cast processing. The manufacturing steps of the cast processing are shown in Fig. 4, using a gyroid structure.

First, wax models are produced, using a 3D printing process, which are then attached to a casting tree. In the further

Table 1 – Theoretical porosity of the samples.

Sample type	Calculated average porosity [%]
Constant 40	42
Linear 40-80	56
Constant 60	57
Quadratic 40-80	63
Constant 80	76

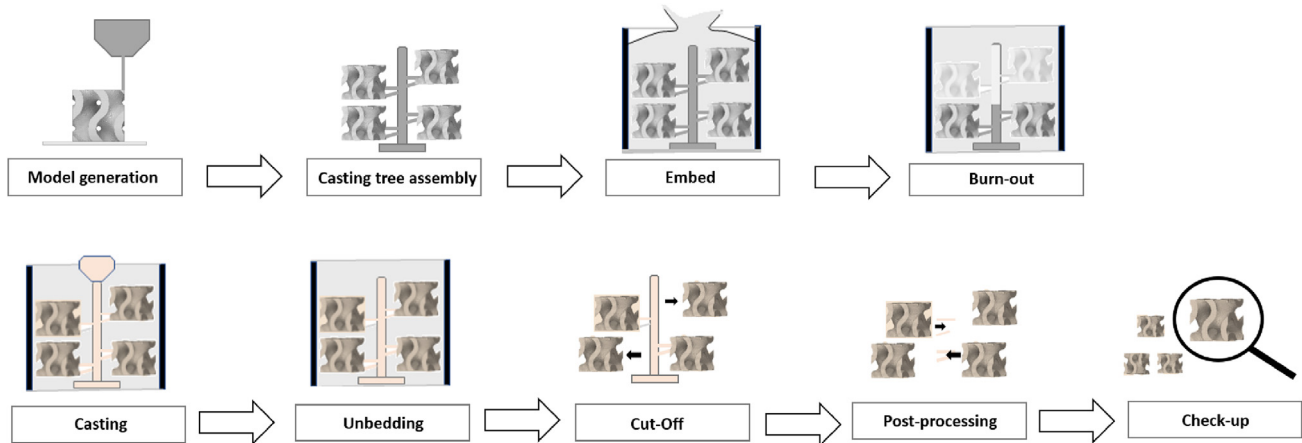


Fig. 4 – Schematic representation of microcast processing, based on a gyroid structure.

manufacturing process, the casting tree with the added components serves as a lost model, in which the structures are embedded in a ceramic mass (in our case gypsum) and burnt out. Then, molten metal is poured into the negative molds, created by the firing process. After the destruction of the ceramic mold, the metal parts can be removed. To achieve complete removal of the investment material in the narrow corridors of the TPMS structure, the structure are first blasted with water. Then the parts are placed in an ultrasonic bath. These two steps are repeated until no investment material is left.

The gyroid structures are manufactured by the company *Nonnenmacher GmbH, Ölbronn Dürm, Germany* and are made of the aluminium alloy *AlSi7Mg0.6* ($\rho = 2,68 \text{ g/cm}^3$, $E = 59 \text{ GPa}$). Fig. 5 shows the surface of the computer-generated model of the gyroid structure with a linear gradient and porosities from 80% to 40%, compared to the corresponding cast model. This shows that the cast is so accurate that the model and the cast can merge seamlessly.

Each casting structure has sprue points from the connection to the casting tree, which are marked in the casting gyroid cube with a linear gradient, shown in Fig. 6. These casting points must be taken into account during the subsequent component inspection.

The presence of the sprue points partially explains why some samples are slightly heavier than the theoretically calculated weight, as shown in Table 2. Table 2 shows the theoretical and actual weights of the samples and the weight

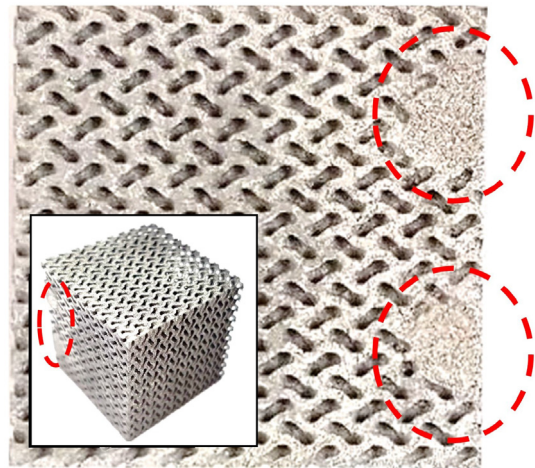


Fig. 6 – Gyroid casting structure with marked sprue points from the casting tree.

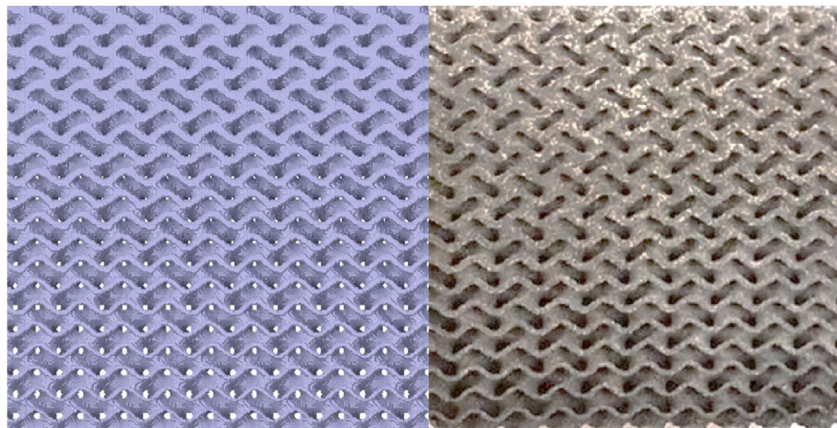


Fig. 5 – Computer-based model compared to the cast model of a gyroid structure, with a linear porosity from 80% to 40%.

deviation in percent. Here, the actual weight of the samples either deviates positively, if the sample is heavier than the theoretical weight, or negatively, if the actual weight is lighter than the theoretical weight.

When considering the theoretical and actual weight of the samples, the largest percentage difference of about (–) 28% is found at the constant porosity of 80%. However, since these samples are also in the low weight range, a percentage deviation of 28% means an absolute value of 2.1 g. Taking these values into account, the manufacturing process provides test samples with a good quality. For the gyroid structures with a constant porosity of 80%, the samples all deviate negatively from the theoretical weight. This is due to the fact that, because of their filigree structure, the edges and corners have already broken off before the test (see Fig. 7).

In contrast, a positive deviation is consistently observed for the gyroid structure with a constant porosity of 40%, which means that the specimens are heavier than their theoretical value. This may be due to the sprue points, as the visual inspection did not reveal any significant gypsum residues in the structure. The uniform structure with a porosity of 60% shows the least variation. For the structures with a linear and a quadratic porosity, the deviations from the theoretical values are sometimes negative and sometimes positive.

4. Testing

To investigate the energy absorption capacity, compression tests were carried out with the machine ‘inspekt 200’, from the company ‘Hegewald & Peschke’. For all specimens, the

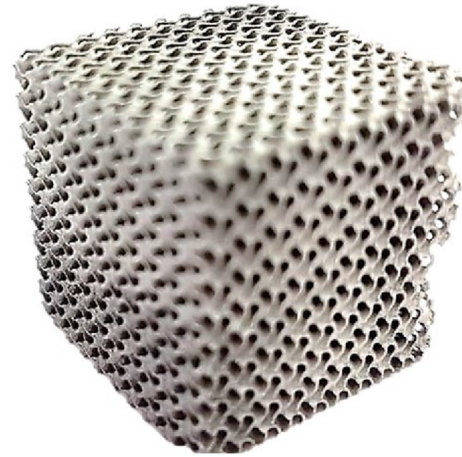


Fig. 7 – Missing mass substance of the gyroid structure with a constant porosity of 80%.

crosshead speed was 0.025 mm/s (initial length (25 mm) * compression speed ($10^{-3}s^{-1}$)). Five gyroid structures of each type were tested. The specimens were placed on the lower pressure plate, so that the sprue points were rested vertically on the plate. The compression tests of the structures with a constant porosity of 40% had to be stopped prematurely, because the punch of the machine got into a one-sided oblique position and wedged. Therefore, it was not possible to calculate the energy absorption capacity of these samples. The wedging during the compression test is shown in Fig. 8.

Table 2 – Theoretical and actual weight of the samples.

Sample type	Sample number	Theoretical weight [g]	Actual weight [g]	Deviation [%]
Constant 40	P1	24.03	24.71	2.82
	P2	24.03	24.78	3.12
	P3	24.03	24.87	3.50
	P4	24.03	24.95	3.83
	P5	24.03	25.49	6.08
Linear 40-80	P1	18.42	17.52	–4.89
	P2	18.42	18.70	1.52
	P3	18.42	17.72	–3.80
	P4	18.42	17.74	–3.69
	P5	18.42	17.92	–2.71
Constant 60	P1	17.77	16.89	–5.21
	P2	17.77	17.74	–0.17
	P3	17.77	17.77	0.00
	P4	17.77	17.05	–4.22
	P5	17.77	17.80	0.17
Quadr. 40-80	P1	15.45	16.10	4.21
	P2	15.45	14.47	–6.77
	P3	15.45	15.30	–0.98
	P4	15.45	15.91	2.98
	P5	15.45	15.68	1.49
Constant 80	P1	9.91	9.28	–6.79
	P2	9.91	8.17	–21.30
	P3	9.91	9.13	–8.54
	P4	9.91	8.83	–12.23
	P5	9.91	7.81	–26.88

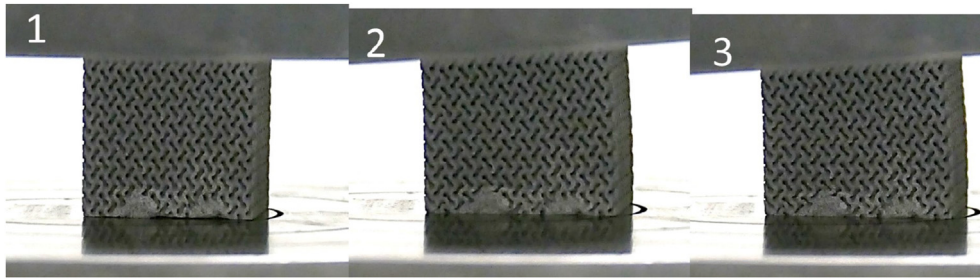


Fig. 8 – Course of the compression test (gyroid; constant 40%): 1. Initial state; 2. Unilateral fracture; 3. Wedging.

5. Results and discussion

The results of the compression test of the stress–strain diagram are shown in Fig. 9. The figure shows five samples for each gyroid type (see Table 2).

As mentioned above, no statement about the energy absorption capacity could be made for the structures with a low porosity (40%), because the mechanical tests had to be stopped before reaching the first peak, due to a one-sided failure of the samples. However, statements can be made about the layer collapse in the stress–strain diagrams. Compared to the other structures, the layer collapse occurred more frequently and in a more intense form, even before reaching the first peak of 50%, which is shown in the stress–strain curve, by the sudden drop in stress. In the other structures, the layer collapsed after this peak. In the gyroid structures with constant porosities of 80% and 60%, minor cell collapses are regularly observed on the plateau. Minor stress drops are also evident in the gradient structures. In Fig. 10, a

structure of each gyroid type is shown for better clarity and the layer collapse is marked.

Ashby's [38] observation that the initial loading curve is not linear can be shared for all samples. This is due to the fact that some cells already fail at low loads. In addition, Ashby describes that an ideal energy absorber is characterised by its long plateau (a long, flat stress–strain curve). In use cases, the plateau stress should be less than the stress of the object being protected [38]. According to the ISO 13314:2011 standard [36], the energy absorption per unit is calculated from the area under the curve up to a strain of 50%, as shown in the following equation (4):

$$W = \int_{\epsilon=0}^{\epsilon(50\%)} \sigma(\epsilon) d\epsilon \quad [\text{MJ}/\text{m}^3] \quad (4)$$

The cumulative energy absorption per unit volume, W , is composed of the strain ϵ [%] and the corresponding stress σ [MPa] during the compression test. According to Ashby, the samples with a constant porosity of 80% and 60% show the

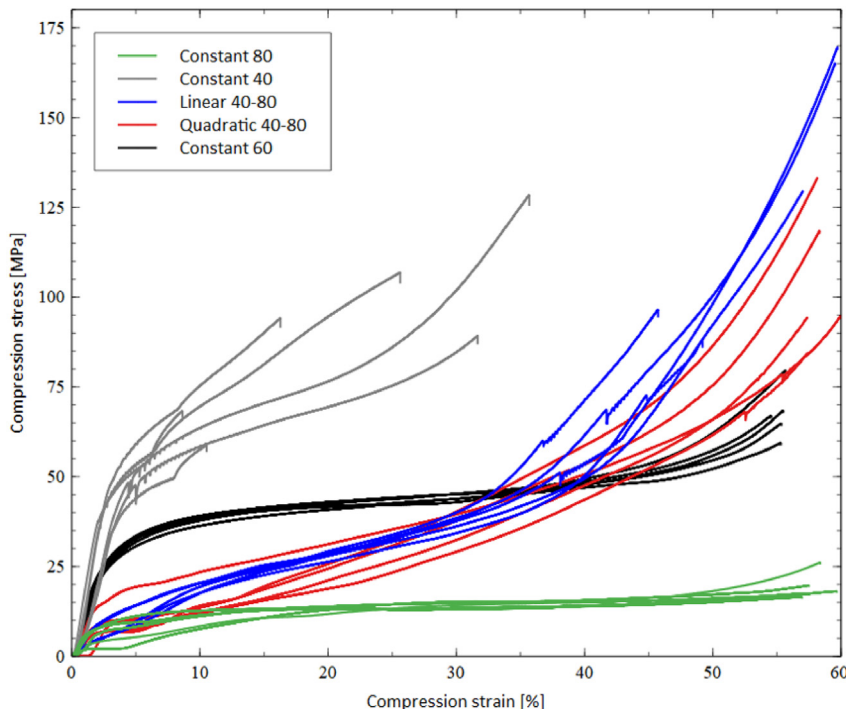


Fig. 9 – Stress–strain diagram of tested structures.

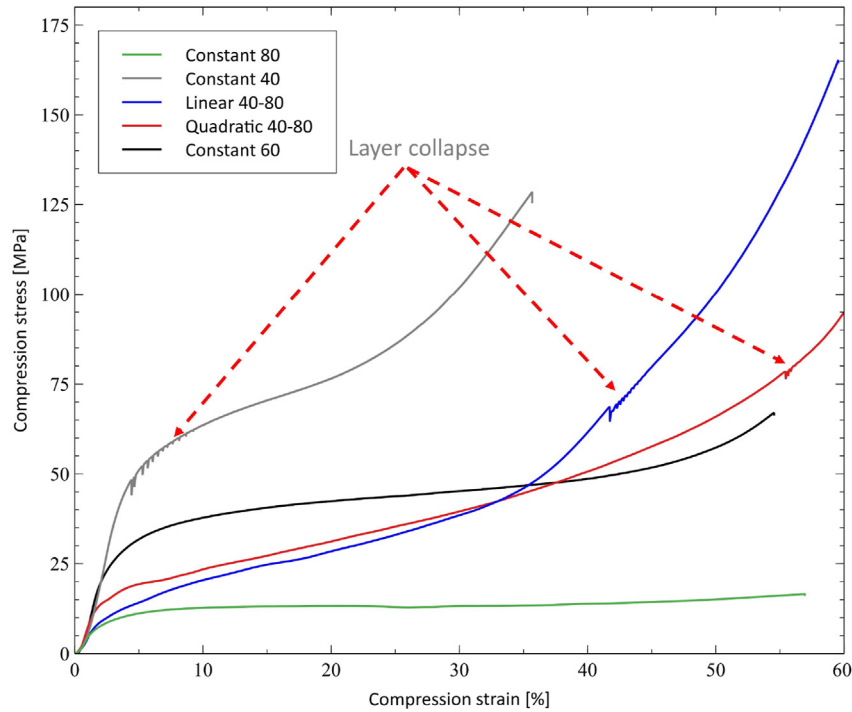


Fig. 10 – Stress–strain diagram - Layer collapse.

ideal course of an energy absorber. The function curve of gyroid structures with a quadratic and linear plateau is not as clearly visible, but has a higher energy absorption potential. Table 3 shows the calculated energy absorption per unit volume. In addition, the mean value of the total samples is given. It is noticeable that there is an outlier upwards, in the value of

the energy absorption of each of the 5 samples, which is written in bold in Table 3.

The samples with a constant porosity of 80% show the lowest energy potential capacity, followed by the samples with a porosity of 60%. The samples with a quadratic and linear curve have the highest energy absorption capacity of the samples listed. When considering the average values, the linear sample has a 40% higher energy absorption capacity, compared to the quadratic sample. However, it should be noted that the quadratic sample has a higher porosity, which is listed in Table 1. The most meaningful comparison is made between the uniform gyroids ‘constant 60’ and the linear gyroids, since these lie in the same porosity range. When considering the average values, the energy absorption capacity at a strain of 50% is more than three times lower for the uniform gyroids ‘constant 60’ than for the linear gyroids. The different curves of the energy absorption capacity can be found in Fig. 11, which plots the cumulative energy absorption per unit volume, W , versus strain. Furthermore, the graph is divided into 4 regions. In the respective strain range, each region is dominated by the energy absorption capacity of a different structure.

It can be observed that area I [from 0% to approx. 12%] shows the highest energy absorption of the uniform gyroids ‘constant 60’, while interval II [from approx. 12%–20%] shows a dominant linear structure, which is followed by the quadratic structure. In the last interval IV [from 35% to 50%], the linear structure dominates again. The good energy absorption in the lower strain range of the constant structure can be explained by its rapid plateau increase in the stress–strain diagram 9. All samples initially have a flat, almost linear region. The linear region of the quadratic and linear samples ends after reaching a compressive load of

Table 3 – Theoretical and actual weight of the samples.

Sample type	Sample number	Energy absorption [MJ/m ³]
Constant 80	P1	309.1
	P2	116.1
	P3	256.4
	P4	155.2
	P5	150.2
	av.	197.4
Constant 60	P1	560.4
	P2	951.9
	P3	745.0
	P4	648.1
	P5	760.7
	av.	733.22
Linear 40-80	P1	2554.7
	P2	2593.8
	P3	3086.8
	P4	3037.5
	P5	2879.4
	av.	2830.44
Quadr. 40-80	P1	1103.7
	P2	1734.4
	P3	1838.9
	P4	2091.3
	P5	1475.8
	av.	1648.82

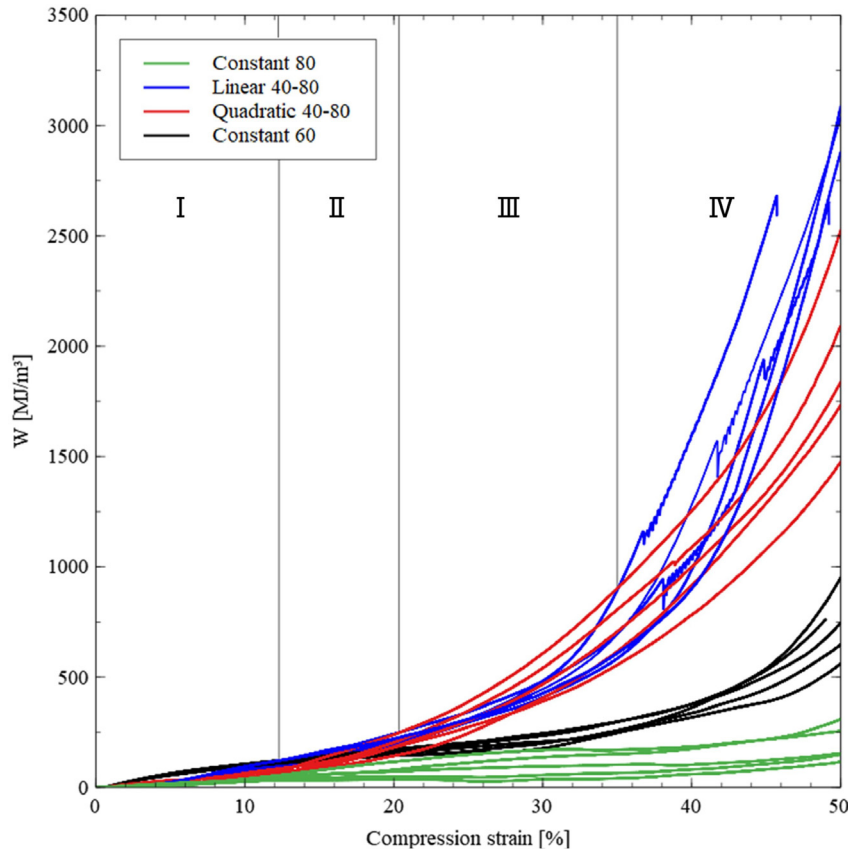


Fig. 11 – Cumulative energy absorption per unit and strain [%].

about 5%, while the linear region of the samples with a constant porosity of 80% is longer. In the work of Dawei Li [18], it was also found that the linear region of the samples with linear gradients is hardly present. This is due to the more pronounced plateau of the samples with a constant porosity of 80%, shown in the stress–strain diagram 9. When looking at the curves of ‘quadratic 40–80’ and ‘linear 40–80’, it can be seen that they are very similar. However, from the beginning of region IV, the energy absorption of the linear sample increases more rapidly. This can be explained by the fact that the linear sample thickens faster, compared to the quadratic sample, which leads to more stability earlier.

The failure modes of the structures are compared in Fig. 12. The structures with a constant porosity show a different failure pattern than the structures with gradients.

For the gyroid structures with a constant porosity of 80%, diagonal shear is a failure mode, as shown in Fig. 12. This observation has also been made by Maskery [17] and by Chenxi Lu [39]. They have investigated (sheet-based) gyroid structures made of an aluminium alloy (Al–Si10–Mg), produced by selective laser sintering (SLS). In the linear (c) and quadratic (d) gyroid structures of Fig. 12, the layered planes with the higher porosity are compressed like an accordion,

while the cells in the lower part of the low porosity samples appear to be unaffected by the forces. This type of failure can be confirmed by the simulation results of the study by Wallat et al. [35]. The simulations were performed in the linear deformation domain, using the simulation software PACE3D. The gyroid structures with linear and quadratic gradients are unit cell structures. It was shown that the stress occurs on the side with the highest porosity, while the structures with a constant porosity show similarly distributed stresses on both sides. In addition, the simulations showed that the ‘linear 40–80’ and ‘quadratic 40–80’ gyroid structures have a higher maximum von Mises equivalent stress than the ‘constant 60’ structures. However, the ‘constant 60’ structures have a higher normalised von Mises stress than the structures with a gradient. Since the lower part of the structures with gradients was not destroyed (see Fig. 12 c, d), it can be concluded from the visual observation of the samples and the simulation results that the structure has more unstressed areas in the parts where the porosity is lower. These overlapping results confirm that simulations in the linear deformation domain can show a trend towards a unit cell structure, which allows to make a basic statement about the failure of the multicellular structure.

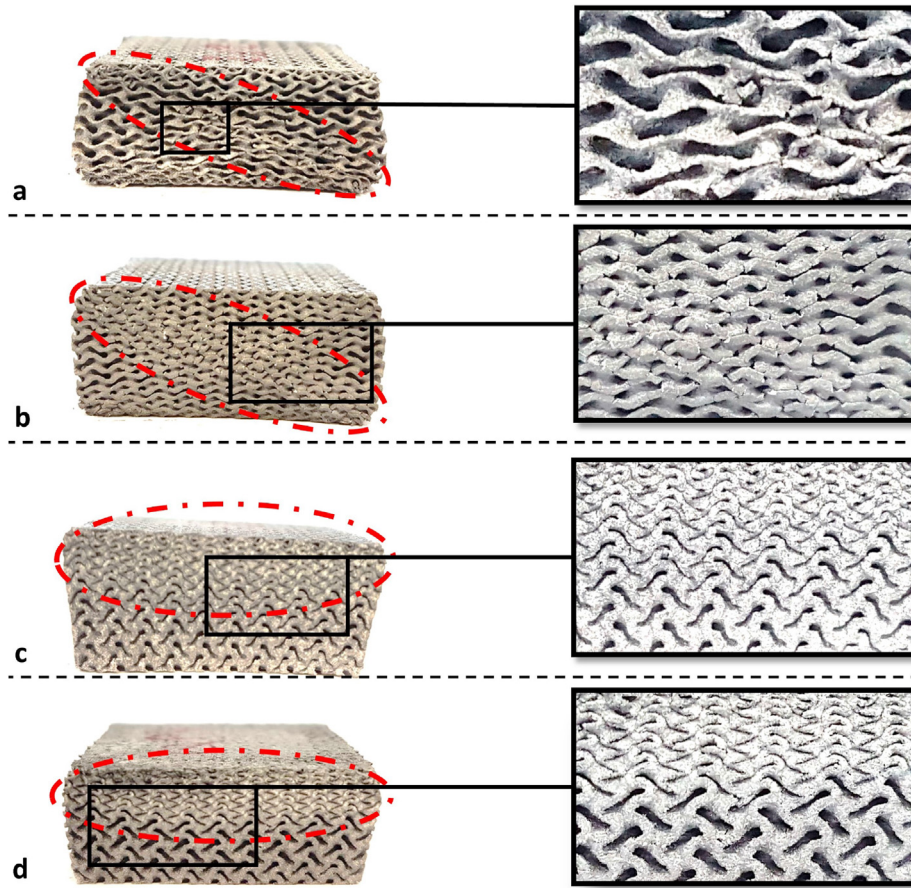


Fig. 12 – Failure modes of gyroid structures - (a) constant 80% and (b) constant 60%: diagonal shear failure; (c) linear gradient 40–80% and (d) quadratic gradient 40–80%: compression in higher porosity area.

6. Conclusions

In this paper, gyroid structures with different gradient profiles (constant, linear and quadratic) were considered and their energy absorption capacity was analysed. For this purpose, the structures were manufactured from an aluminium alloy, using microcast processing, which represents an alternative manufacturing option for complex structures. Compression tests were performed and evaluated to investigate the energy absorption capacity. With regard to the energy absorption capacity, the following could be shown:

- I The gyroid structures with a constant porosity of 80% and 60% have a more significant plateau, but the energy absorption capacity is significantly lower than that of the linear and quadratic gradient structures.
- II Overall, the samples with a linear gradient performed best, in terms of energy absorption. These samples were found to have three times the energy absorption capacity, compared to the samples with a constant porosity of 60%.
- III The samples with a constant porosity of 60% show the best energy absorption potential in the lower strain range [0% - 12%].

- IV The samples with a quadratic gradient have good energy absorption in the medium strain range [20% - 35%].
- V After the compression tests, the individual cells of the constant samples were visibly more damaged than those of the samples with a linear and quadratic gradient.
- VI In the range of linear deformation, simulations of a unit cell structure can show a trend for a fundamental statement about the failure of a multicellular structure.

These results indicate the high potential of structures with gradients and open up the possibility of achieving the desired energy absorption capacity in the future, by optimising the topology of the gyroid structure. Adaptation to the energy absorption capacity is a central issue in vehicle safety. The gradient structure creates a new lightweight construction and design option with new potential. In addition, the gradient makes it possible to adapt a porous structure to its environment. This is interesting in the field of tissue engineering, when a porous structure needs to be adapted to the bone structure.

In the future, the performance of using the structures with gradients as cores for devices will be a crucial issue of further research. Yin [40] has integrated TPMS structures with constant porosity into square tubes to demonstrate a reinforcing

energy absorber. This study could be extended to structures with gradients.

Furthermore, variation of the gradient functions enable for a digital design of tailored porous structures specifically developed for particular applications.

In order to be able to make a more precise statement about the transferability of unicellular to multicellular structures, an investigation of the homomorphism of the gyroid structures is a future research topic.

A detailed microstructure characterization and the determination of phase composition under the processing conditions of inert atmosphere as well as possible effects on the mechanical properties are addressed in forthcoming studies of microcast processing.

Data availability

The stl files of the structures as well as the simulative and experimental results of the study are freely available in the software Kadi4Mat. Kadi4Mat [41] is an open-source software developed at the Institute for Applied Materials - Microstructure Modelling and Simulation (IAM-MMS) of the Karlsruhe Institute of Technology (KIT). It is mainly used to manage research data in the field of materials science. This should make the exchange between scientists more transparent and easier.

Declaration of Competing Interest

The authors declare that they have no known competing financial interests or personal relationships that could have appeared to influence the work reported in this paper.

Acknowledgement

The paper was written as part of the project “InSeL - Innovative Schaumstrukturen für den effizienten Leichtbau” (Innovative foam structures for efficient lightweight construction), which is funded by the European Regional Development Fund (ERDF) and the state of Baden-Wuerttemberg, as part of the Center for Applied Research ZAFH. A continuation of the work was possible thanks to the project “Mittelbau” funded by the ministry of the state of Baden-Wuerttemberg. We are very grateful to all participating sponsors. Furthermore, the authors thank Leon Geisen for his editorial support.

REFERENCES

- [1] Schaedler Tobias A, Carter William B. Architected cellular materials. *Annu Rev Mater Res* 2016;46(1):187–210. <https://doi.org/10.1146/annurev-matsci-070115-031624>.
- [2] Bodaghi M, Serjouei A, Zolfagharian A, Fotouhi M, Rahman H, Durand D. Reversible energy absorbing meta-sandwiches by FDM 4D printing. *Int J Mech Sci* 2020;173:105451. <https://doi.org/10.1016/j.ijmecsci.2020.105451>. ISSN 0020–7403.
- [3] Saba Matthias, Wilts Bodo D, Hielscher Johannes, Schröder-Turk Gerd E. Absence of circular polarisation in reflections of butterfly wing scales with chiral gyroid structure. *Mater Today Proc* 2014;1:193–208. <https://doi.org/10.1016/j.matpr.2014.09.023>. ISSN 2214–7853. – Living Light: Uniting biology and photonics – A memorial meeting in honour of Prof Jean-Pol Vigneron.
- [4] Yan Chunze, Hao Liang, Yang Lei, Hussein Ahmed, Young Philippe, Li Zhaoqing, Li Yan. Design of TPMS structures 2021:27–38. <https://doi.org/10.1016/B978-0-12-824438-8.00002-9>. ISBN 9780128244388.
- [5] Fan Xiaojie, Tang Qian, Feng Qixiang, Ma Shuai, Song Jun, Jin Mengxia, Guo Fuyu, Jin Peng. Design, mechanical properties and energy absorption capability of graded-thickness triply periodic minimal surface structures fabricated by selective laser melting. *Int J Mech Sci* 2021;204:106586. <https://doi.org/10.1016/j.ijmecsci.2021.106586>. ISSN 0020–7403.
- [6] Park So-Yeon, Kim Kyu-Sik, AlMangour Bandar, Grzesiak Dariusz, Lee Kee-Ahn. Compressive deformation behavior and energy absorption characteristic of additively manufactured sheet CoCrMo triply periodic minimal surface lattices. *J Mater Res Technol* 2022;18:171–84. <https://doi.org/10.1016/j.jmrt.2022.02.086>. ISSN 2238–7854.
- [7] Al-Ketan Oraib, Rowshan Reza, Abu Al-Rub Rashid K. Topology-mechanical property relationship of 3D printed strut, skeletal, and sheet based periodic metallic cellular materials. *Addit Manuf* 2018;19:167–83. <https://doi.org/10.1016/j.addma.2017.12.006>. ISSN 2214–8604.
- [8] Liu Hailong, Ahlinder Astrid, Yassin Mohammed A, Finne-Wistrand Anna, Gasser TC. Computational and experimental characterization of 3D-printed PCL structures toward the design of soft biological tissue scaffolds. *Mater Des* 2020;188:108488. <https://doi.org/10.1016/j.matdes.2020.108488>. ISSN 0264–1275.
- [9] Khrapov Dmitriy, Kozadayeva Maria, Manabaev Kayrat, Panin Alexey, Sjöström William, Koptyug Andrey, et al. Different approaches for manufacturing Ti-6Al-4V alloy with triply periodic minimal surface sheet-based structures by electron beam melting. *Materials* 2021;14(17). <https://doi.org/10.3390/ma14174912>. ISSN 1996–1944.
- [10] Fina Fabrizio, Goyanes Alvaro, Madla Christine M, Awad Atheer, Trenfield Sarah J, Kuek Jia M, Patel Pavanesh, Gaisford Simon, Basit Abdul W. 3D printing of drug-loaded gyroid lattices using selective laser sintering. *Int J Pharm* 2018;547(1):44–52. <https://doi.org/10.1016/j.ijpharm.2018.05.044>. ISSN 0378–5173.
- [11] Dong Zhifei, Zhao Xin. Application of TPMS structure in bone regeneration. *Engineered Regeneration* 2021;2:154–62. <https://doi.org/10.1016/j.engreg.2021.09.004>. ISSN 2666–1381.
- [12] Al-Ketan Oraib, Rezgui Rachid, Rowshan Reza, Du Huifeng, Fang Nicholas X, Abu Al-Rub Rashid K. Microarchitected stretching-dominated mechanical metamaterials with minimal surface topologies. *September Adv Eng Mater* 2018;20(9). <https://doi.org/10.1002/adem.201800029>. ISSN 1438–1656.
- [13] Jin Yuan, Kong Haoyu, Zhou Xueyong, Li Guangyong, Du Jianke. Design and characterization of sheet-based gyroid porous structures with bioinspired functional gradients. *Materials* 2020;13(17). ISSN 1996–1944, <https://www.mdpi.com/1996-1944/13/17/3844>.
- [14] Kapfer Sebastian C, Hyde Stephen T, Mecke Klaus, Arns Christoph H, Schröder-Turk Gerd E. Minimal surface scaffold designs for tissue engineering. *Biomaterials* 2011;32(29):6875–82. <https://doi.org/10.1016/j.biomaterials.2011.06.012>. ISSN 0142–9612.
- [15] Higuera S, Miralbes R, Ranz D. Mechanical properties and energy-absorption capabilities of thermoplastic sheet gyroid

- structures. *O Mech Adv Mater Struct* 2021;1–15. <https://doi.org/10.1080/15376494.2021.1919803>. O.
- [16] Downing David, Jones Alistair, Brandt Milan, Leary Martin. Increased efficiency gyroid structures by tailored material distribution. *Mater Des* 2021;197:109096. <https://doi.org/10.1016/j.matdes.2020.109096>. ISSN 0264–1275.
- [17] Maskery I, Sturm L, Aremu AO, Panesar A, Williams CB, Tuck CJ, Wildman RD, Ashcroft IA, Hague RJM. Insights into the mechanical properties of several triply periodic minimal surface lattice structures made by polymer additive manufacturing. *Polymer* 2018;152:62–71. <https://doi.org/10.1016/j.polymer.2017.11.049>. ISSN 0032–3861. – SI: Advanced Polymers for 3DPrinting/Additive Manufacturing.
- [18] Li Dawei, Liao Wenhe, Dai Ning, Xie Yi M. Comparison of mechanical properties and energy absorption of sheet-based and strut-based gyroid cellular structures with graded densities. *Materials* 2019;12(13). <https://doi.org/10.3390/ma12132183>. ISSN 1996–1944.
- [19] Liu Fei, Mao Zhongfa, Zhang Peng, Zhang David Z, Jiang Junjie, Ma Zhibo. Functionally graded porous scaffolds in multiple patterns: new design method, physical and mechanical properties. *Mater Des* 2018;160:849–60. <https://doi.org/10.1016/j.matdes.2018.09.053>. ISSN 0264–1275.
- [20] Maskery I, Aboulkhair NT, Aremu AO, Tuck CJ, Ashcroft IA. Compressive failure modes and energy absorption in additively manufactured double gyroid lattices. *Addit Manuf* 2017;16:24–9. <https://doi.org/10.1016/j.addma.2017.04.003>. ISSN 2214–8604.
- [21] Garboczi E, Bentz D, Martys N. *Experimental Methods for porous media*. 1. Academic Press; 1999 (Digital images and computer modelling). – ISBN 0–12–475982–3.
- [22] Yang Nan, Wei Huaxian, Mao Zhongfa. Tuning surface curvatures and young's moduli of TPMS-based lattices independent of volume fraction. *Mater Des* 2022;216:110542. <https://doi.org/10.1016/j.matdes.2022.110542>. ISSN 0264–1275.
- [23] Khaleghi Saeed, Dehnavi Fayyaz N, Baghani Mostafa, Safdari Masoud, Wang Kui, Baniassadi Majid. On the directional elastic modulus of the TPMS structures and a novel hybridization method to control anisotropy. *Mater Des* 2021;210:110074. <https://doi.org/10.1016/j.matdes.2021.110074>. ISSN 0264–1275.
- [24] Gibson Lorna J, Ashby Michael F. *Cellular solids: Structure and properties*. 2 (Cambridge Solid State Science Series). Cambridge University Press; 1997. <https://doi.org/10.1017/CBO9781139878326>.
- [25] Alketan Oraib, Abu Al-Rub Rashid. Multifunctional mechanical-metamaterials based on triply periodic minimal surface lattices: a review. *Adv Eng Mater* 2019;(7). <https://doi.org/10.1002/adem.201900524>.
- [26] Li Weihong, Yu Guopeng, Yu Zhibin. Bioinspired heat exchangers based on triply periodic minimal surfaces for supercritical CO₂ cycles. *Appl Therm Eng* 2020;179:115686. <https://doi.org/10.1016/j.applthermaleng.2020.115686>. ISSN 1359–4311.
- [27] Abueidda Diab W, Elhebeary Mohamed, Shiang Cheng-Shen, Pang Siyuan, Abu Al-Rub Rashid K, Jasiuk Iwona M. Mechanical properties of 3D printed polymeric Gyroid cellular structures: experimental and finite element study. *Mater Des* 2019;165:107597. <https://doi.org/10.1016/j.matdes.2019.107597>. ISSN 0264–1275.
- [28] Shi Xin, Liao Wenhe, Li Peifeng, Zhang Changdong, Liu Tingting, Wang Cong, Wu Jiajing. Comparison of compression performance and energy absorption of lattice structures fabricated by selective laser melting. *Adv Eng Mater* 2020;22(11):2000453. <https://doi.org/10.1002/adem.202000453>.
- [29] Yu Jason, Sun Jinxing, Bai Jiaming. Investigation of functionally graded TPMS structures fabricated by additive manufacturing. *Mater Des* 2019;182(7):108021. <https://doi.org/10.1016/j.matdes.2019.108021>.
- [30] Zhang Junfang, Shen Yifan, Sun Yuanxi, Yang Jianxing, Gong Yu, Wang Ke, Zhang Zhiqing, Chen Xiaohong, Bai Long. Design and mechanical testing of porous lattice structure with independent adjustment of pore size and porosity for bone implant. *J Mater Res Technol* 2022;18:3240–55. <https://doi.org/10.1016/j.jmrt.2022.04.002>. ISSN 2238–7854.
- [31] Ma Xiangyu, Zhang David, Zhao Miao, Jiang Junjie, Luo Fangqiong, Hailun Zhou. Mechanical and energy absorption properties of functionally graded lattice structures based on minimal curved surfaces. *Int J Adv Manuf Technol* 2022;118(1). <https://doi.org/10.1007/s00170-021-07768-y>.
- [32] Baykasoglu Cengiz, Cetin Merve T. Energy absorption of circular aluminium tubes with functionally graded thickness under axial impact loading. *Int J Crashworthiness* 2015;20(1):95–106. <https://doi.org/10.1080/13588265.2014.982269>.
- [33] Abramowicz W. Thin-walled structures as impact energy absorbers. *Thin-Walled Struct* 2003;41(2):91–107. [https://doi.org/10.1016/S0263-8231\(02\)00082-4](https://doi.org/10.1016/S0263-8231(02)00082-4). ISSN 0263–8231. – Buckling strength and Failure Mechanics of Thin walled structures.
- [34] [matlab. version 9.6.0.1072779 \(R2019a\)](https://www.mathworks.com/). Natick, Massachusetts: The MathWorks Inc.; 2019.
- [35] Wallat Leonie, Altschuh Patrick, Reder Martin, Nestler Britta, Poehler Frank. Computational design and characterisation of gyroid structures with different gradient functions for porosity adjustment. *Materials* 2022;15(10). <https://doi.org/10.3390/ma15103730>. ISSN 1996–1944.
- [36] [International Organization for Standardization. Mechanical testing of metals - ductility testing - compression test for porous and cellular metals](https://www.iso.org/standard/68411.html). Geneva: CH; Dezember 2011. Standard.
- [37] Hällgren Sebastian, Pejryd L, Ekengren Jens. 3D data export for additive manufacturing - improving geometric accuracy. *Procedia CIRP* 2016;50(12):S. 518–523. <https://doi.org/10.1016/j.procir.2016.05.046>.
- [38] Ashby MF, Evans T, Fleck NA, Hutchinson JW, Wadley HNG, Gibson LJ. *Metal foams: a design guide*. Elsevier Science; 2000. ISBN 9780080511467, <https://books.google.de/books?id=C0daIBo6LjgC>.
- [39] Lu Chenxi, Zhang Chi, Wen Pin, Chen Fei. Mechanical behavior of Al–Si10–Mg gyroid surface with variable topological parameters fabricated via laser powder bed fusion. *J Mater Res Technol* 2021;15:5650–61. <https://doi.org/10.1016/j.jmrt.2021.11.008>. ISSN 2238–7854.
- [40] Yin Hanfeng, Tan Dingwen, Wen Guilin, Tian Wanyi, Wu Qiankun. Crashworthiness analysis and optimization design of TPMS-filled structure. *Int J Crashworthiness* 2021;1–18. <https://doi.org/10.1080/13588265.2021.1959171>.

- [41] Brandt Nico, Griem Lars, Herrmann Christoph, Schoof Ephraim, Tosato Giovanna, Zhao Yinghan, Zschumme Philipp, Selzer Michael. Kadi4Mat : a research data infrastructure for materials science. S. Art.–Nr.: 8 Data Sci J 2021;20(1). <https://doi.org/10.5334/dsj-2021-008>. ISSN 1683–1470. – 43.31.01; LK 01.



Leonie Wallat is a research associate at the “Institute of Materials and Processes” and the Institute “Digital Materials Science” at Karlsruhe University of Applied Sciences. Since the end of 2020, she has been engaged in research on TPMS structures. Enclosed

you will find the link: <https://www.h-ka.de/die-hochschule-karlsruhe/organisation-personen/personen-a-z/person/leonie-wallat-1>



Dr.-Ing. Michael Selzer is group leader of the department “Multiscale Materials Modelling and Data Processing” at the Institute for Applied Materials Computational Materials Science (IAM-CMS) (Karlsruher University of Applied Sciences, KIT). Enclosed you will find the link: https://www.iam.kit.edu/mms/english/Mitarbeiter_selzer.php



Prof. Dr.-Ing. Uwe Wasmuth is Head of Applied Materials Science of University of Applied Science. Enclosed you will find the link: <https://www.h-ka.de/en/imp/profile/applied-materials-science>



Prof. Dr.-Ing. Frank Poehler is Vice Dean and Dean of Studies for the Mechanical Engineering Bachelor's program of University of Applied Science. His area of expertise is in polymerengineering. Enclosed you will find the link to his homepage: <https://www.h-ka.de/en/about-hka/organization-people/staff-search/person/frank-michael-poehler>



Prof. Dr. rer. nat. Britta Nestler is Professor for Microstructure Simulation in Materials Engineering at Karlsruhe University of Applied Sciences. Enclosed you will find her website and more information about her publications: https://www.iam.kit.edu/mms/Mitarbeiter_nestler.php